Case study and climatological analysis of upper tropospheric jet stream and stratosphere-troposphere exchanges using VHF profilers and radionuclide measurements in France

Jean-Luc Baray, Yves Pointin, Joël van Baelen, Marie Lothon, Bernard Campistron, Jean-Pierre Cammas, Olivier Masson, Aurélie Colomb, Claude Hervier, Yannick Bezombes, et al.

Case Study and Climatological Analysis of Upper-Tropospheric Jet Stream and Stratosphere–Troposphere Exchanges Using VHF Profilers and Radionuclide Measurements in France

JEAN-LUC BARAY,[a] YVES POINTIN,[a] JOËL VAN BAELEN,[a] MARIE LOTHON,[b] BERNARD CAMPISTRON,[b] JEAN-PIERRE CAMMAS,[c] OLIVIER MASSON,[d] AURÉLIE COLOMB,[a] CLAUDE HERVIER,[a] YANNICK BEZOMBES,[b] SANDRA BANSON,[a] CHRISTOPHE DUROURE,[a] DANY HADAD,[a] AND FRÉDÉRIC TRIDON[e]

[a] *Laboratoire de Météorologie Physique, UMR6016, Observatoire de Physique du Globe de Clermont-Ferrand, Clermont-Ferrand, France*
[b] *Laboratoire d'Aérologie, UMR5560, Observatoire Midi-Pyrénées, Toulouse, France*
[c] *Laboratoire de l'Atmosphère et des Cyclones, UMR8105, OSU-Réunion, Saint Denis de la Réunion, France*
[d] *Institut de Radioprotection et de Sûreté Nucléaire, Saint Paul lez Durance, France*
[e] *Earth Observation Sciences, Department of Physics and Astronomy, University of Leicester, Leicester, United Kingdom*

(Manuscript received 27 October 2016, in final form 24 August 2017)

ABSTRACT

The authors present a climatological analysis of tropospheric horizontal wind profiles and jet stream events using long series of wind profiles from two VHF profilers located in France: Lannemezan (2001–14) and Opme (1999–2014). A case study of jet stream and stratospheric intrusion of air into the troposphere that occurred in January 2013 is first described and demonstrates the capability of the VHF profilers to detect jet stream events. The climatology study over the two sites reveals the strongest values of seasonal wind during winter (21.4 m s^{-1} at 8.7-km height at Opme; 25.1 m s^{-1} at 9.6-km height at Lannemezan). A methodology based on the automatic detection of maximum winds on a decadal series of hourly wind profiles allows the detection of jet stream events and establishes its climatology for each site. A frequency analysis of jet stream events of westerly winds over 50 m s^{-1} presents a clear seasonality at the two sites, with a maximum in winter (3.5%–9.7% of hourly profiles) and a minimum in summer (near 1%). Cosmogenic radionuclides sampled at Opme also exhibit a clear seasonal variation with maximum in spring and minimum in the cold seasons; the ^{7}Be/^{22}Na activity ratio confirms stratosphere-to-troposphere exchanges for the studied cases. The mean interannual variability of the frequency of jet stream events is 1.5% in Opme and 2.9% in Lannemezan. Positive decadal trends are observed for the two sites: +1.6 ± 1.2% decade^{-1} for Opme and +2.4 ± 2.2% decade^{-1} for Lannemezan.

1. Introduction

Jet streams are strong zonal winds in the upper troposphere, identified in the first half of the twentieth century by observing the motions of clouds (Schaefer 1953). The jet streams are caused by the combination of Earth's rotation on its axis and atmospheric heating by solar radiation. Palmin and Newton (1948) showed the coincidence between the jet stream's maximum wind and tropopause discontinuities, paving the way to numerous studies of dynamical coupling and exchanges between the stratosphere and the troposphere (Shapiro 1980; Ancellet et al. 1991; Holton et al. 1995; Baray et al. 1998; Trickl et al. 2011; Ivanova 2016). Krishnamurti (1961) distinguished two eastward jet streams in the upper troposphere of the Northern Hemisphere: the subtropical jet stream located at the poleward edge of the Hadley cell, and the polar jet stream, farther poleward. Jet streams are dynamical processes that are concentrated in zones of maximum wind speed that strongly influence mesoscale meteorology. For example, shifts in the polar-front jet stream patterns are linked to the severe winter of 2009/10 in northwestern Europe and the eastern United States (Cattiaux et al. 2013; Cohen et al. 2010; Fereday et al. 2012), and to the wet British summer of 2007 (Blackburn et al. 2008). Analyzing the relationship between the European blocking and jet stream north–south shift, Davini et al. (2014) showed

Corresponding author: Dr Jean-Luc Baray, j.l.baray@opgc.fr

DOI: 10.1175/JAMC-D-16-0353.1

that the majority of blocking events influence the westerlies above the Atlantic Ocean and are associated with their poleward displacement. The subtropical jet stream can enhance the deep-layer vertical shear of the horizontal wind and inhibit intense hurricanes (Bukunt and Barnes 2015).

In the global climate change context, the long-term evolution of the jet stream strength and location remains uncertain. Based on the European Centre for Medium-Range Weather Forecasts (ECMWF) ERA-40 and NCEP reanalyses from 1979 to 2001, Archer and Caldeira (2008a,b) found that jet streams have risen in altitude, moved poleward, and globally weakened, with some local and seasonal exceptions. Strong and Davis (2007, 2008) found slightly different results, with jet core speeds increasing above the midlatitudes. Degirmendžić and Wibig (2007) performed a complex classification of jet stream patterns in Europe and noticed that most jet stream types produce day-to-day changes of the wind field, indicating an enhancement of circulation dynamics in the upper troposphere. Barnes and Polvani (2013) documented how the midlatitude jet stream responds to climate change using model output from CMIP5. They also found that climate change induces a poleward migration of jet streams and a change of the pattern variability.

Direct observations of jet streams using very high frequency (VHF) Doppler radar made it possible to identify and to document the dynamics of jet streams (Thomas et al. 1986; Yoe and Rüster 1992). Fukao et al. (1991) used 2 years of VHF radar observations to examine the average vertical velocity profiles near the jet stream wind maximum. However, to our knowledge, no recent publications document the evolution of jet streams using decadal direct observations. This is the purpose of this study, focusing on jet stream events characterized by westerly winds greater than $50\,\mathrm{m\,s^{-1}}$.

Two French VHF profiler radars were installed in Lannemezan (43.1°N; 0.4°E) and Opme (45.7°N; 3.1°E) in the 1990s and have been operated almost continuously through the present time. This instrumentation is useful to describe dynamical processes and to establish upper-tropospheric local wind climatologies. The data from these locations are assimilated in global models within the framework of the European E-Profile network, a European Meteorological Services Network (EUMETNET) observation program (Haefele et al. 2014), and could be used for satellite validation, such as the future satellite mission of the European Space Agency Atmospheric Dynamics Mission Aeolus (ADM-Aeolus; Reitebuch et al. 2009).

A number of observational studies have demonstrated the feasibility of using cosmogenic radionuclide measurements to estimate the presence of stratospheric air at ground level (Leppänen et al. 2012; Steinmann et al. 2013). Because some such measurements are routinely sampled at Opme and Lannemezan, their concentrations will be studied to develop a jet stream climatology.

In this paper, after describing the instruments, datasets, and methodology, we present a case study of jet streams and stratosphere–troposphere exchange observed above the two sites. Climatology and decadal trends of wind and jet stream frequency over the two measurement sites are then presented, analyzed, and compared with stratosphere–troposphere exchanges from radionuclide measurements.

2. The instrumentation, data, and model analyses

a. VHF profiler radars

Radio waves are scattered by turbulence in the atmosphere. Remote sensing of atmospheric parameters is based on the analysis of backscattered waves. Wind profiles by radars depend on the scattering of electromagnetic energy by minor irregularities in the index of refraction, which is related to the speed at which electromagnetic energy propagates through the atmosphere. When an electromagnetic wave encounters a refractive index irregularity, part of its energy is scattered in all directions. Backscattering occurs preferentially from irregularities of a size on the order of one-half the wavelength of the incident wave. Because the refractive index fluctuations are advected by the background wind, they can be used as tracers. Tropospheric winds can be measured by VHF profilers that use the Doppler frequency shift of signals scattered from atmospheric turbulence to monitor wind profiles from near the surface to the lower stratosphere (Ecklund et al. 1979). The Opme and Lannemezan radars are clear-air Doppler wind VHF profiler radars (Fig. 1).

The pulse peak power is 4.5 kW for the Opme system, and 6 kW for Lannemezan. For both systems, the transmitter frequency is 45.0 MHz, and the pulse repetition frequency is 6.4 kHz. The antenna field is made of two perpendicular sets of 60-m coaxial–collinear lines fed with or without fixed delay, enabling the radar beam to be successively pointed vertically, and at 15° off the vertical in four oblique beams, depending on a control sequence. For each of the five beams, the radial velocity is estimated from the Doppler frequency shift. This allows the measurement of the time evolution of the vertical profiles of the three wind components and of the atmospheric reflectivity observed in the five directions, with a radial resolution of 375 m and a time resolution of 15 min.

The vertical wind measurement is directly calculated from the vertical beam. The uncertainty of the vertical wind is then only associated to the variability of the signal-to-noise ratio (SNR) and to the statistical variability of the

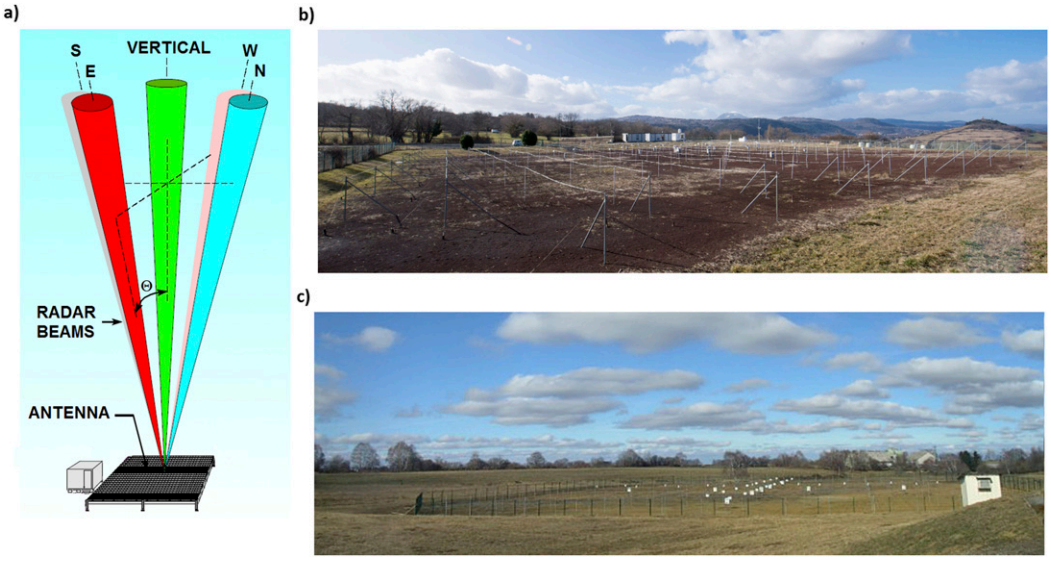

FIG. 1. (a) Schematic representation of a VHF wind profiler. Photographs of the systems at (b) Opme (copyright by LaMP@CNRS photothèque Cyril Fresillon), and (c) Lannemezan (copyright by Solène Derrien).

Doppler measurement. This has been estimated to be on the order of 1 cm s^{-1}, (Nastrom et al. 1990). The error must actually increase with altitude (since the SNR decreases) but remains generally low and will increase abruptly when the SNR approaches 0 dB.

The horizontal wind is determined from a combination of inclined radar beams. Hence, the uncertainty can be more important because of the hypothesis on the uniformity of the wind field between these different beams. According to Strauch et al. (1987), Adachi et al. (2005), and Rao et al. (2008), these errors vary according to the method used (two, three, or four shots) but is on the order of 1–2 m s^{-1}. The measurement uncertainty is therefore negligible in comparison.

For this study, hourly averaged data were used. After being installed at Aubière (close to Clermont-Ferrand) from December 1990 to December 1995, the system was moved to Opme, a rural site about 10 km away from the center of Clermont-Ferrand and at 660 m above sea level. The number of days of operation by year and month of both systems is given in Tables 1 and 2.

With three other French VHF radars located in Toulon, Toulouse, and at the Observatoire de Haute Provence, these two systems were used previously for several studies of tropospheric dynamics, including the tropopause folding (Caccia and Cammas 1998; Bertin et al. 2001), variations of the tropopause height (Kim et al. 2001), atmospheric tides (Diaz de Argandona et al. 2010), and also a sky-mapping study (Campistron et al. 2001). They were deployed for the field campaigns the Pyrenees Experiment (PYREX; Bougeault et al. 1990), the Mesoscale Alpine Program (MAP; Petitdidier et al. 1997), and the Stratosphere–Troposphere Exchanges, Meso-Scale Investigations (in French) (ESTIME; Caccia et al. 2000). Lannemezan and Opme are the two last VHF radars of this network still in operation.

b. *Radionuclide measurements*

The cosmogenic radionuclides attached to aerosols were also studied, and their variation was compared with dynamical parameters measured with VHF radars. Aerosols have been sampled in Opme since 2006 and in Lannemezan since 2014 using a homemade sampler developed by IRSN and operating at 335 $m^3 h^{-1}$. The aerosol sampler is equipped with a four-layer polypropylene fiber filter (JPE 13160; Jonell, Inc.) to ensure a high collection efficiency (minimum of about 95% for particles with an aerodynamic diameter of 30 nm). Aerosol filters were measured by gamma spectrometry on low-background high-purity germanium (HPGe) detectors. The studied cosmogenic radionuclides are easily quantified based on gamma-ray emissions at 477.6 and 1274.5 keV, respectively. Relative error does not exceed 10%. Radionuclide measurements are sampled on a weekly basis. Among the numerous cosmogenic radionuclides, we focus on beryllium-7 (^{7}Be; half-life = 53.3 days) and sodium-22 (^{22}Na; half-life = 2.6 yr). Their production is localized in the upper troposphere and lower stratosphere. They result from interactions (named spallation reactions) of high-energy particles (mostly protons) with light atmospheric nuclei, that is, oxygen and nitrogen atoms in the case of ^{7}Be or argon in the case of ^{22}Na (Tokuyama and Igarashi 1998). Cosmogenic radionuclides rapidly attach to submicrometer aerosols, by which they are transported to the ground-level air (Arnold

TABLE 1. VHF radar dataset: number of days of operation by year for each site.

	Opme		Lannemezan	
	Days of operation	Hourly profiles	Days of operation	Hourly profiles
1998	3	68		
1999	195	4432		
2000	324	7489		
2001	306	7103	202	4493
2002	353	8449	358	8429
2003	359	8446	364	8630
2004	359	8429	363	8649
2004	363	8606	359	8436
2006	281	6560	337	7978
2007	355	8364	309	7216
2008	366	8866	39	912
2009	365	8518	336	7720
2010	363	8594	233	5285
2011	360	8517	229	5286
2012	252	5718	217	5134
2013	298	6924	359	8470
2014	174	3970	356	8442

and Al-Salih 1955). Their stratospheric concentrations are generally one to two orders of magnitude greater than corresponding ground-level concentrations (about some millibecquerels per meter cubed for ^{7}Be and some microbecquerels per meter cubed for ^{22}Na). There exists a large scientific literature devoted to ^{7}Be that can be easily quantified thanks to their high concentration levels in the air (from thousand to tens of thousands of microbecquerels per meter cubed). Regarding ^{22}Na, the number of studies is rather small because the detection requires a combination of high volume sampling and low-background gamma spectrometer. ^{22}Na was only determined in Opme because the flow rate of the sampler in Lannemezan was too low to exceed the detection limits for ^{22}Na. ^{7}Be and ^{22}Na have been recognized as powerful tracers of tropospheric downdrafts or springtime stratosphere–troposphere exchanges (Cristofanelli et al. 2006; Jasiulionis and Wershofen 2005; Steinmann et al. 2013) and are both used in aerosol transport modeling from the stratosphere to ground-level air (Feely et al. 1989; Peters 1959; Tokuyama and Igarashi 1998).

c. *ERA-Interim, trajectories, and reverse domain filling*

In our study, we use also parameters extracted from the ERA-Interim reanalysis archive produced by ECMWF. Several horizontal resolutions have been used: 1° for back-trajectory computations, 0.25° in latitude and longitude for synoptic fields and 0.125° for profiles at the grid point nearest the sites. The temporal resolution is 6 h (0000, 0600, 1200, and 1800 UTC). The parameters are extracted for 37 pressure levels between 1 and 1000 hPa. ERA-Interim is the reanalysis of the period 1989 to the present that has replaced the ERA-40 archive. The main advances in the ERA-Interim data assimilation relative to ERA-40 are the 12-h 4D variational analysis, the T255 horizontal original resolution, improvement in the humidity analysis, model physics and data quality control, variational bias correction of satellite radiance data, and other improvements in bias handling (Dee et al. 2011).

To determine the origin of the air masses, we calculated kinetic 3D back trajectories with the "LACYTRAJ" trajectory model (Clain et al. 2010) with a 15-min time step. The resolution of ERA-Interim is sometimes too coarse to highlight subgrid-scale structures; therefore, we calculated vertical cross sections of potential vorticity with 48-h advection using the reverse domain-filling technique code based on LACYTRAJ (LACYTRAJ-RDF). This approach consists of running back trajectories with a regular gridded array, then interpolating the tracer to back-trajectory points, and finally copying values forward to regular grid; this insures improvement of the vertical resolution and retrieval of subgrid information that was not in the initial field (Dritschel 1988). LACYTRAJ and LACYTRAJ-RDF have previously been used to study stratosphere–troposphere exchange in the southern subtropics (Clain et al. 2010), monsoon depressions (Baray et al. 2010), long-range interhemispheric transport of carbon monoxide (Duflot et al. 2010), or interactions between the mixing layer and the free troposphere (Freney et al. 2016).

3. Example of jet stream and stratosphere–troposphere exchange

Before documenting the climatology of jet streams, we present an illustrative case study. Our motivation is to describe the dynamical processes during a jet stream event that occurred above western Europe in January 2013 and which was observed at the two sites.

TABLE 2. VHF profiler dataset: number of days of operation by month for each site.

Month	Opme radar	Lannemezan radar
1	420	322
2	409	264
3	468	324
4	432	295
5	458	290
6	413	345
7	407	382
8	378	375
9	401	346
10	451	372
11	412	351
12	426	395

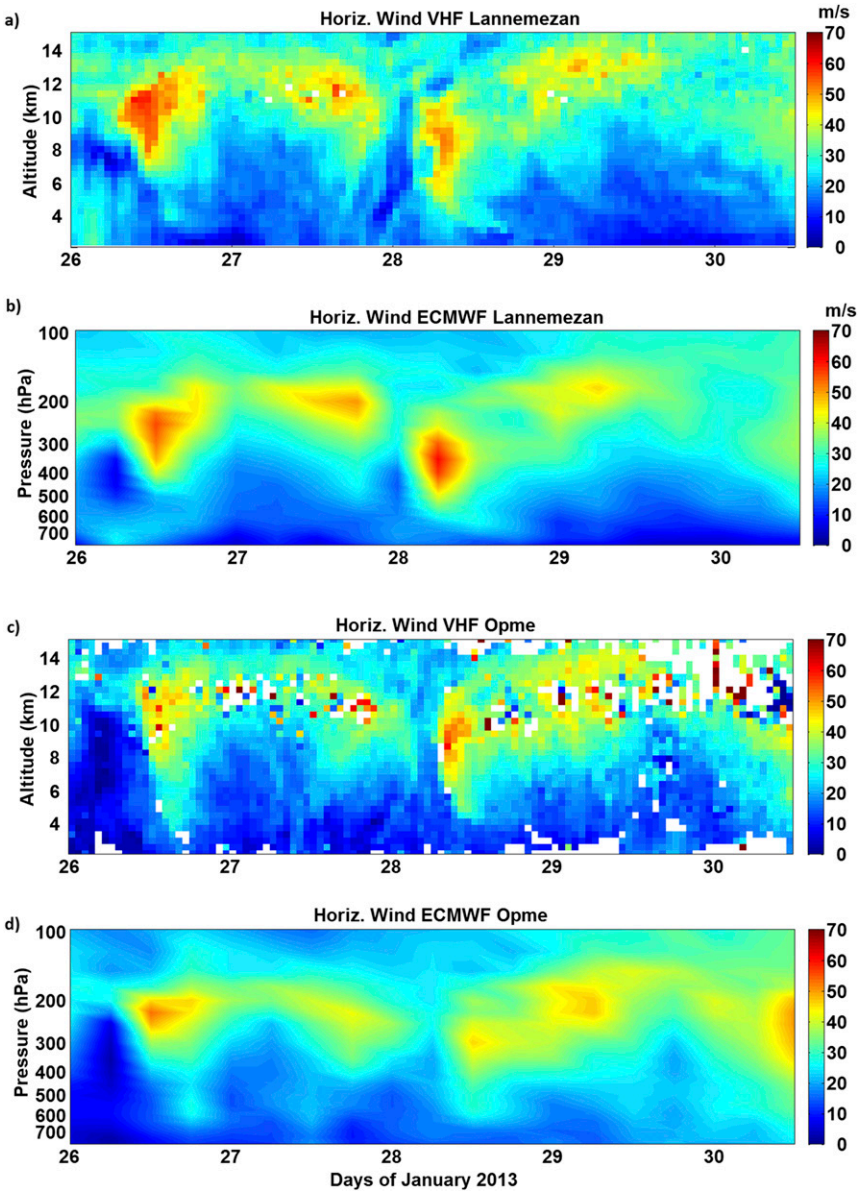

FIG. 2. Hourly averaged horizontal wind speed profile ($m\,s^{-1}$) measured by the VHF profiler above (a) Lannemezan and (c) Opme between 0000 UTC 26 Jan and 1200 UTC 30 Jan 2013, and the ERA-Interim horizontal wind speed profile ($m\,s^{-1}$) for the grid point nearest to (b) Lannemezan and (d) Opme.

Figure 2 gives the temporal evolution of the horizontal wind profiles measured by the VHF radars and compares the two ECMWF grid points nearest Lannemezan (43.125°N, 0.375°E) and Opme (45.75°N, 3.125°E). The maximum horizontal wind is found between 8- and 12-km height during the day of 26 January 2013 and between 6 and 11 km during the day of 28 January 2013. The maximum horizontal wind values observed are $59\,m\,s^{-1}$ at 12 km on 1000 UTC 26 January above Lannemezan and $51\,m\,s^{-1}$ at 9 km on 0900 UTC 28 January above Opme. This upper-tropospheric wind structure corresponds quite well to wind fields given by ERA-Interim, and is of the same order of magnitude, except for the maximum of wind above Opme on 28 January, which is less than $46\,m\,s^{-1}$ in the ERA-Interim. Polar and subtropical jet streams are not continuous westerly wind tubes. They take a wave structure and are made up of jet cores where the wind speed is maximum. The air masses that enter or leave a jet core area are strongly accelerated or decelerated.

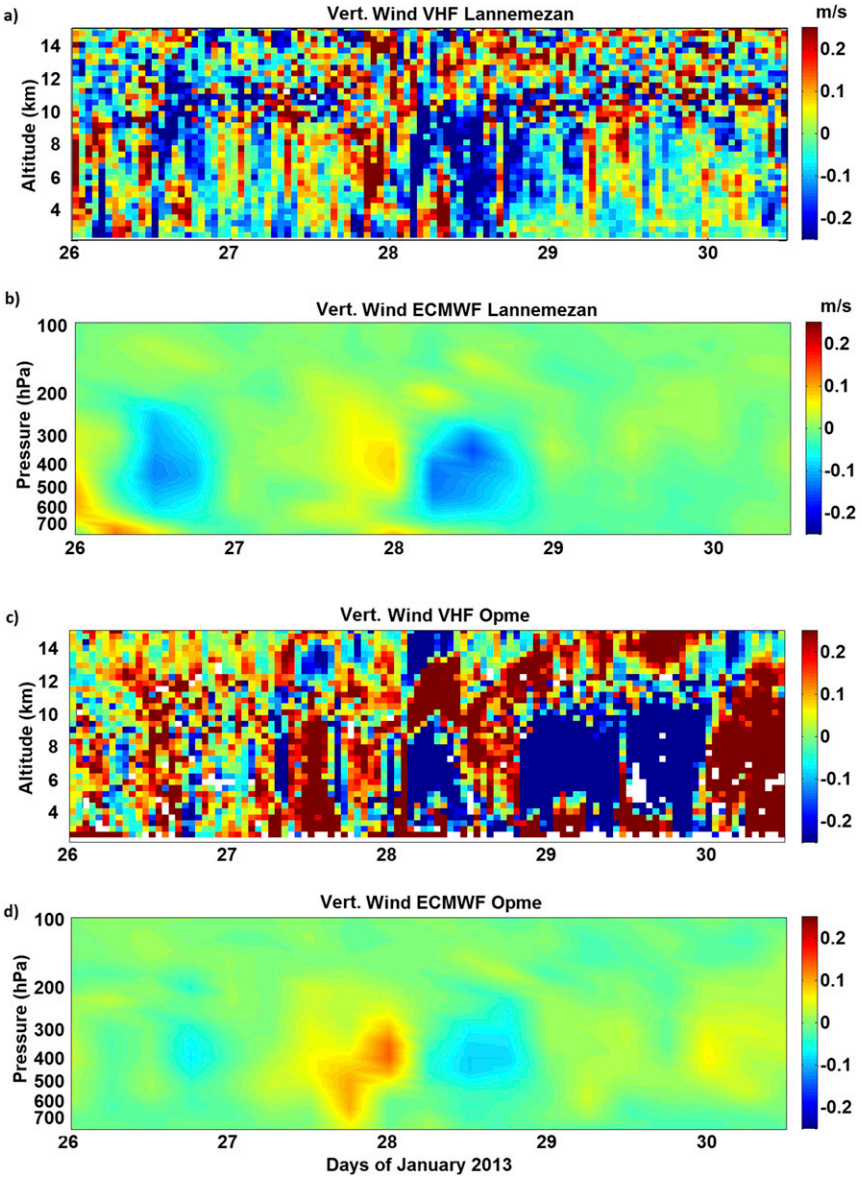

FIG. 3. As in Fig. 2, but for the vertical wind.

The present case is a succession of several jet cores that form above the Atlantic Ocean and are advected westward, giving the jet stream, a Rossby wave structure. Two of them are observed above the two sites on 26 and 28 January. This results in transverse and vertical ageostrophic circulations inducing, in the most intense cases, tropopause folds and stratosphere–troposphere exchanges (Shapiro 1980; Holton et al. 1995).

Figure 3 gives the temporal evolution of the vertical wind profiles measured by the VHF radars and compares the two ECMWF grid points nearest Lannemezan and Opme. Strong vertical winds are indeed observed in the upper troposphere during this period at both sites by VHF radars and ERA-Interim: downdrafts on 28 January in the morning above Opme and Lannemezan and from 2000 UTC 28 January to 2200 UTC 29 January above Opme and updrafts in the evening in Opme and at noon in Lannemezan on 27 January. The ERA-Interim provides also similar vertical wind structures, but with large difference of the wind speed. The time resolution is different (6 vs 1 h) and vertical winds are stronger above Lannemezan for ERA-Interim, but stronger above Opme for the VHF profiler. The agreement between the ERA-Interim and the profiler time series at time scales larger than 6 h is good, particularly for Lannemezan. At shorter time scales, the agreement may deteriorate because the

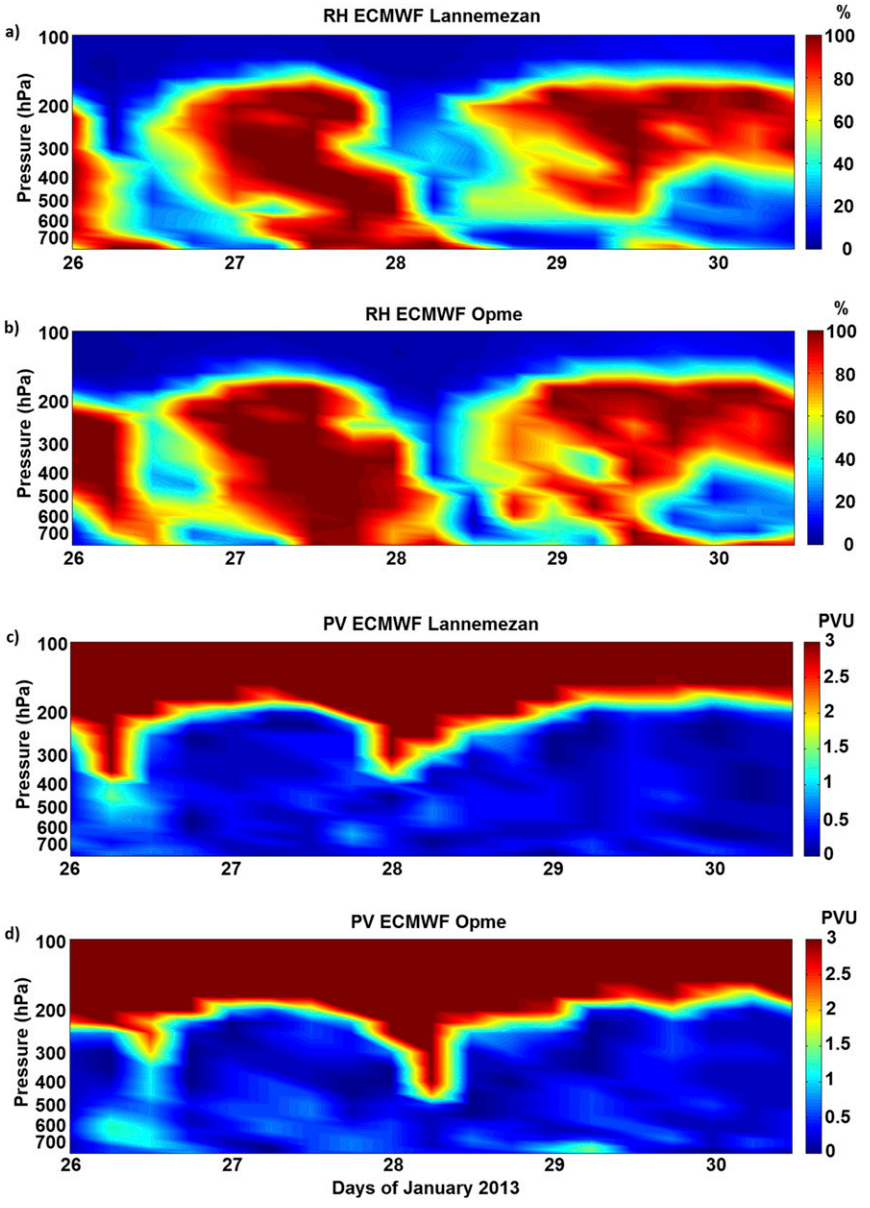

FIG. 4. (a) ERA-Interim relative humidity (%) for the grid point nearest to (a) Lannemezan and (b) Opme between 0000 UTC 26 Jan and 1200 UTC 30 Jan 2013, and ERA-Interim potential vorticity (PVU, 1 PVU = 10^{-6} K m^2 kg^{-1} s^{-1}) for the grid point nearest (c) Lannemezan and (d) Opme.

vertical velocity is the component of the wind that has the largest variability in space and in time. Vertical winds from NCEP reanalysis (not shown) are similar to ERA-Interim vertical winds. The cause of the difference in the vertical wind speeds between observations and global models for this case study is not known.

Figure 4 shows time series of dynamical indicators, the relative humidity and potential vorticity, a tracer of stratospheric air (Staley 1960), for the nearest points from Lannemezan and Opme. They present similar characteristics that suggest subsidence of stratospheric air into the upper troposphere on the morning of 28 January, with low values of relative humidity and high values of potential vorticity.

A Raman lidar providing water vapor mixing ratio profiles has been operational at Aubière since 2009 (Fréville et al. 2015). Figure 5 shows that the water vapor profile obtained during the night between 29 and 30 January presents successive layers of wet air (below 2 km, and between 4 and 5.5 km) and dry air (near 3 km,

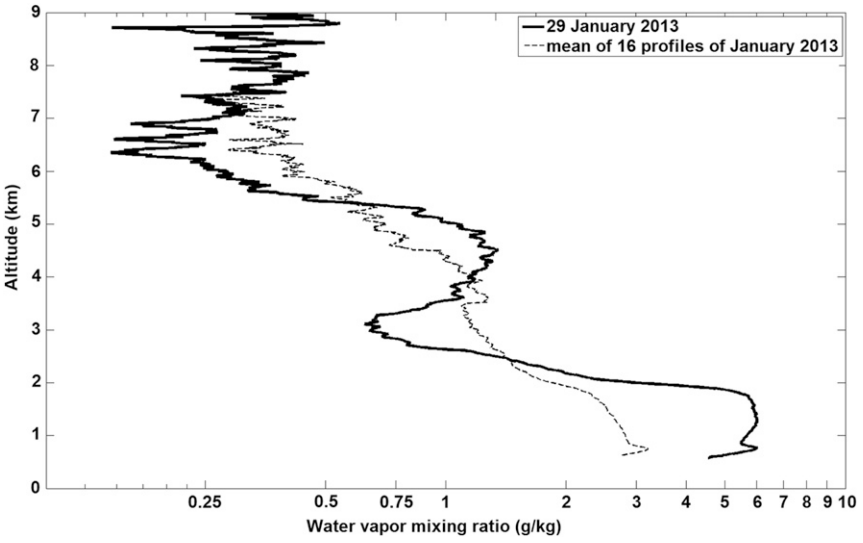

FIG. 5. Water vapor mixing ratio profile ($g\,kg^{-1}$) measured with Raman lidar at Clermont-Ferrand during the night from 29 to 30 Jan 2013 (solid line) compared with the mean of 16 lidar profiles of January 2013 (dashed line).

and above 5.5 km). These values can be compared with the monthly mean water vapor profile obtained by averaging all January profiles for 2013: The two dry layers near 3 km and above 5.5 km show water vapor mixing ratios about 0.70 and 0.25 $g\,kg^{-1}$; this is less than the climatological profiles of about 1.2 and 0.4 $g\,kg^{-1}$ at the corresponding altitude layers. This is to be contrasted with the two wet layers below 2 km and between 4 and 5.5 km that have water vapor mixing ratios near 6 and 3 $g\,kg^{-1}$ as compared with the climatological profiles that have ratios near 3 and 0.9 $g\,kg^{-1}$.

Figure 6 focuses on the 28 January 2013 episode. It presents the evolution of ERA-Interim wind and potential vorticity fields. The wind field confirms the presence of a jet core, and indicates that, on 28 January in the morning, Opme is under the influence of an exit area of a jet core centered on England with a southeast direction. The potential vorticity field displays a stratospheric filament of stratospheric air (more than 6 PVU), passing over Opme on 28 January in the morning.

Figure 7 presents a group of 7-day back trajectories computed using LACYTRAJ and a vertical cross section of potential vorticity advected by back trajectories following the reverse domain-filling method. The stratification of wet and dry layers observed by Raman lidar could be the signature of air masses from different origins, with traces of stratospheric intrusions occurring before the moment of the lidar measurement, at the altitude of dry layers, or during the night of 29 January, but being not well resolved by ERA-Interim. Indeed, the Opme VHF wind profiler detects strong downward motions (more than 1 $m\,s^{-1}$) from 2000 UTC 28 January to 2200 UTC 29 January (Fig. 3c). These subsidences are not observed at Lannemezan, and are also not clearly visible on ERA-Interim winds (Figs. 3a,b,d). The back trajectories indicate a mixing of stratospheric–polar and of lower-tropospheric–oceanic origins for the air masses arriving over Clermont-Ferrand on 0600 UTC 28 January 2013. Finescale cross sections of potential vorticity have been calculated using the reverse domain-filling technique (Fig. 7b). The high values (>2 PVU) near 45°N above 400 hPa, corresponding to 7-km altitude, confirm the stratospheric origin of the dry layer seen by the lidar above 5.5 km. Some finescale bubbles of high values of potential vorticity are also seen near 450 and 550 hPa, consistent with the successive wet and dry layers seen by the lidar, but it is difficult to establish a direct link between them with certainty.

To summarize, in this case study, we show that the two sites can be under the influence of an upper-level jet stream and associated stratospheric intrusions. In addition, in the present case study, a succession of jet cores is observed above the two sites. The Opme and Lannemezan VHF profilers have the capability to detect jet core events, while the Raman lidar in Aubière can detect signatures of stratospheric intrusions in the water vapor profiles.

4. Climatology and trends

a. Seasonal wind profiles

To address the climatological wind behavior of the two sites, we calculated the seasonal profiles in the horizontal wind speed from 1998 to 2014 at Opme (Fig. 8) and from 2001 to 2014 at Lannemezan (Fig. 9). The lower limit of

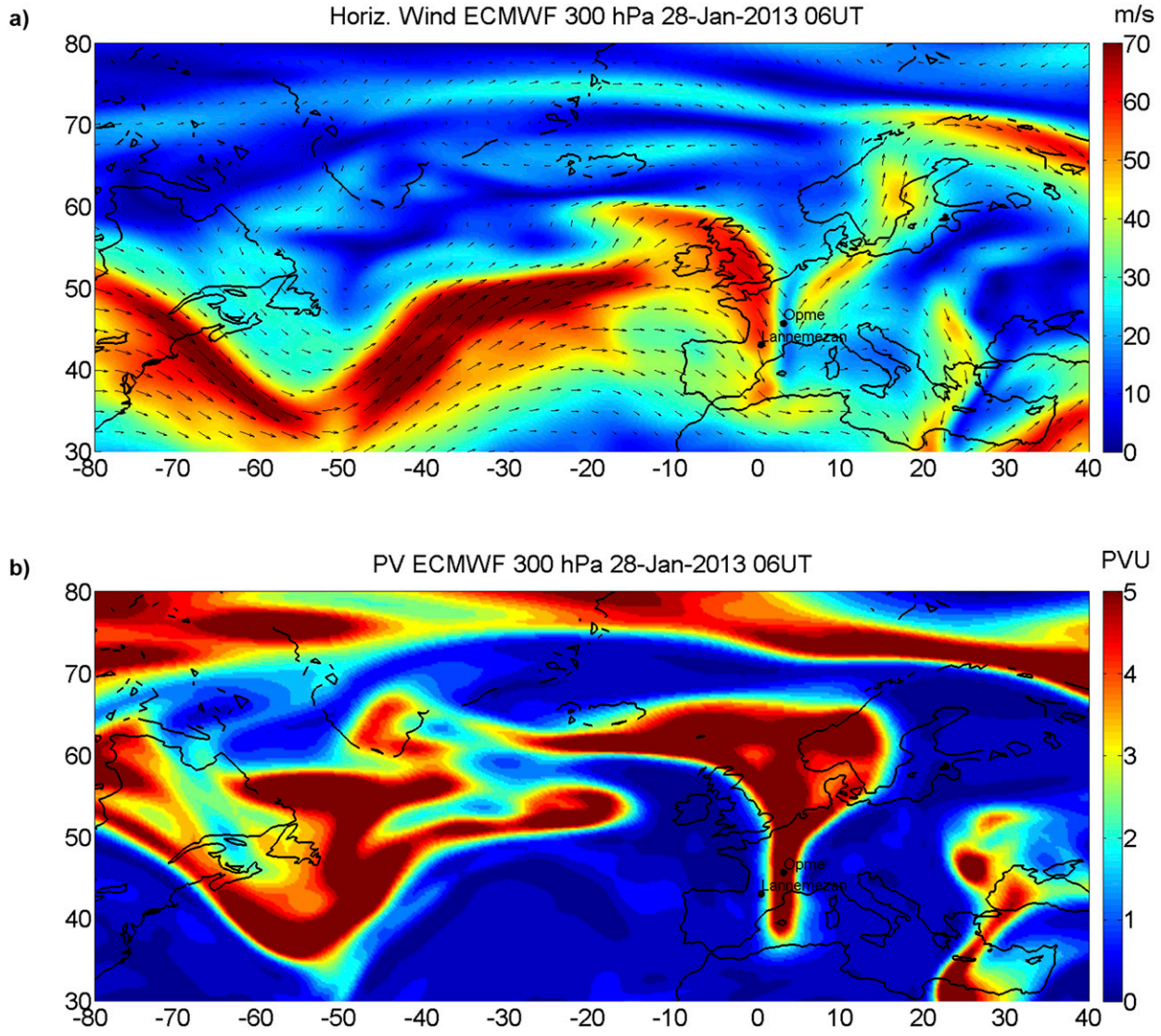

FIG. 6. ERA-Interim (a) horizontal wind ($m\,s^{-1}$) and (b) potential vorticity (PVU) on the 300-hPa surface at 0600 UTC 28 Jan 2013.

the validity domain of the Opme VHF radar is compared with surface winds measured with a sonic anemometer operating at the summit of the puy de Dôme, 1465 m above sea level, and located less than 15 km away from Opme. Both mean values and standard deviation in the wind speeds are consistent with the bottom of the profiles. Above Opme, the strongest values of the seasonal wind speed are obtained during winter reaching 21.4 $m\,s^{-1}$ at 8.7 km, with a standard deviation near 13 $m\,s^{-1}$. For the rest of the year, the maximum wind speed is between 18.3 and 20.4 $m\,s^{-1}$, and located between 8.5- and 10-km height, with a standard deviation slightly lower than in winter. Above Lannemezan, the maximum climatological wind speed is also observed in winter. The wind speed profile has a maximum of 25.1 $m\,s^{-1}$ at 9.6-km height, with a standard deviation near 15 $m\,s^{-1}$. For the other seasons, the maximum is between 21.2 and 21.5 $m\,s^{-1}$ and is located between 10- and 11.5-km height. The ECMWF climatological profiles present a similar structure and seasonality, but with a larger maximum of wind speed, located at a slightly higher altitude: Opme maximum wind is 27.1 $m\,s^{-1}$ at 10.3-km height in winter, 24.2 $m\,s^{-1}$ at 11-km height in summer, and Lannemezan maximum wind is 26.2 $m\,s^{-1}$ in winter, 23.2 $m\,s^{-1}$ in summer, at the same height as Opme. The wind direction calculated from the two horizontal wind components indicates strong westerly winds associated with the polar and subtropical jet streams. Opme, when compared with Lannemezan, shows a smaller maximum wind speed, located at a lower altitude. The wind speed difference between the two sites is less than

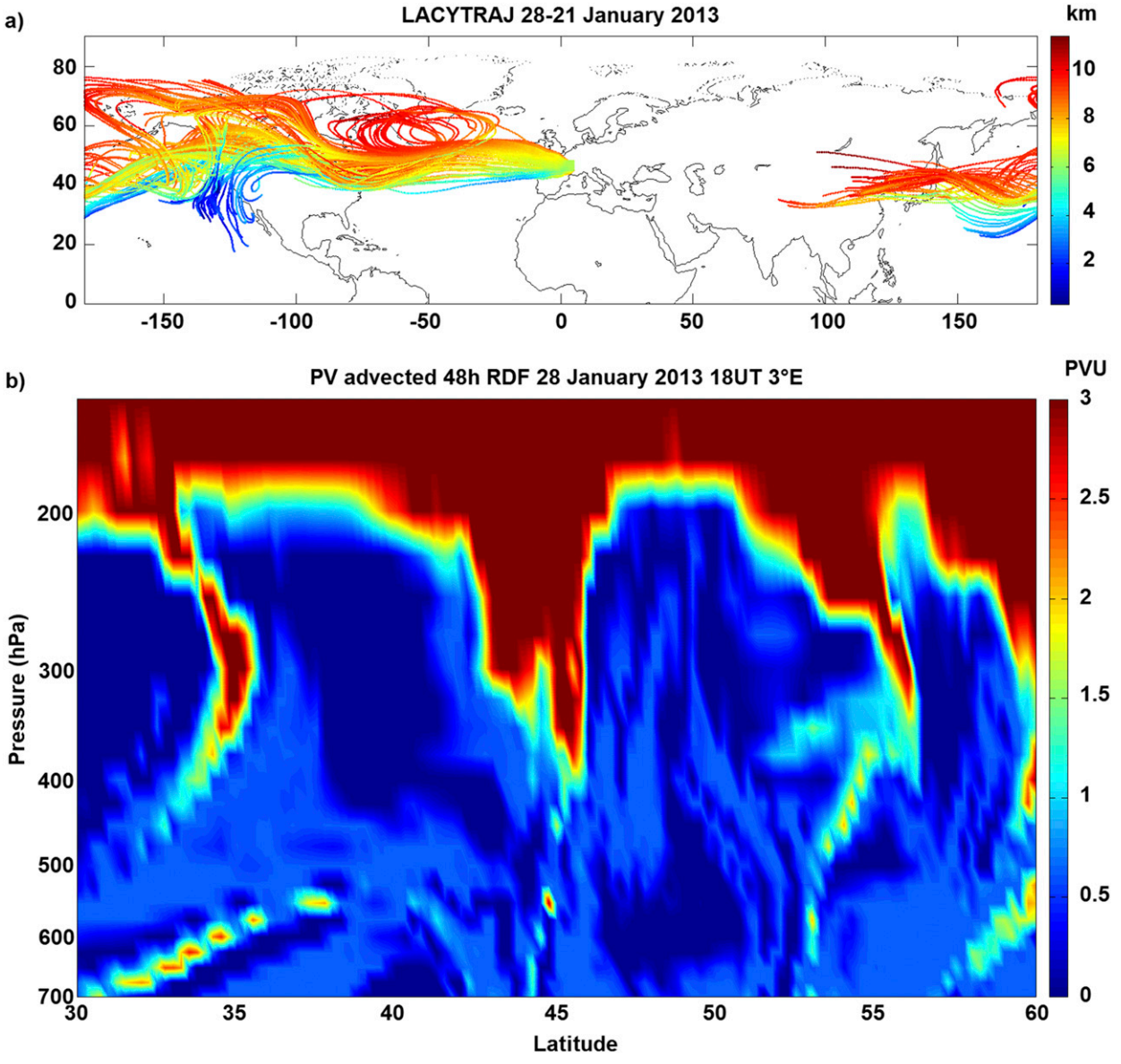

FIG. 7. (a) Seven-day back trajectories arriving over Clermont-Ferrand on the 300-hPa surface at 0600 UTC 28 Jan 2013. The color scale indicates the altitude (km) of the air masses. (b) Vertical cross section of 48-h advected potential vorticity (PVU) at 3°E as a function of pressure level (hPa) at 1800 UTC 29 Jan 2013.

$4\,m\,s^{-1}$, and the altitude difference is less than 1 km. This difference, slightly higher than the measurement uncertainty, is not clearly reproduced by ERA-Interim and could be because of differences in the local topography.

b. *Methodology of detection of jet stream events on VHF radar wind fields*

Despite the continuous improvement of atmospheric models, it remains important to establish climatological distributions and long-term trends of climatic variables from observations. Hence, we exploit the available decadal series of VHF radar wind profiles to automatically detect jet stream events over the stations.

Our methodology is based on the analysis of hourly wind profiles. The detection is based on several criteria: the westerly component must be positive, and the wind speed must be larger than $50\,m\,s^{-1}$. These two criteria have to be fulfilled for two (or more) radar levels, consecutive or not, between 6- and 14-km height, and during 4 h or more. With these criteria, we could detect all identified jet stream events over the stations, after performing sensibility tests with different wind speed and time values.

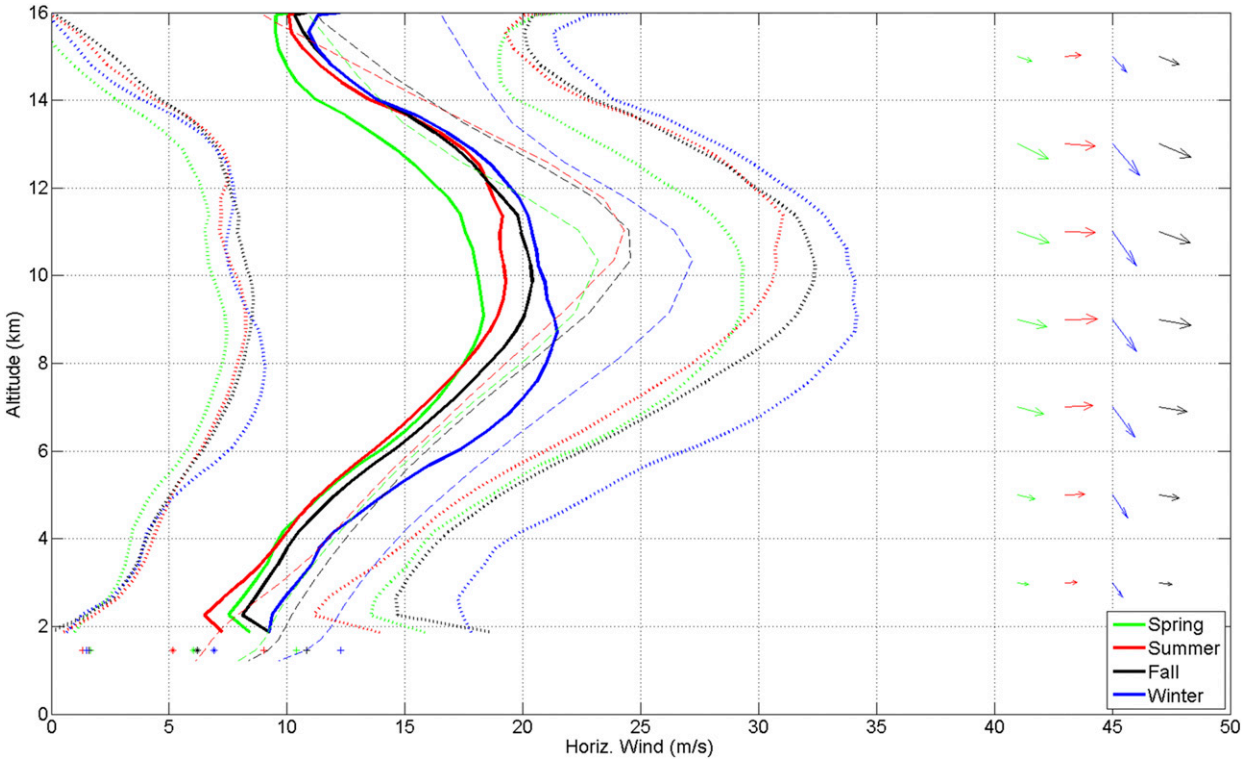

FIG. 8. Climatological profiles from the horizontal wind speed (solid lines) and direction (arrows on the right side) observed with the Opme VHF radar (1998–2014) for spring (green), summer (red), autumn (black), and winter (blue). The dotted lines mark ±1 standard deviation. The dashed lines provide the ERA-Interim climatological profiles for the same period. The plus signs below 2 km indicate the mean and ±1 standard deviation values obtained by the sonic anemometer at the top of the puy de Dôme station.

Jet streams are nonlinear processes in which the wind speed can decrease and increase during a single event. Their shapes can depend on the season: Kuang et al. (2014) showed that upper-tropospheric jet streams frequently have a spiral-like pattern in winter, but a quasi-annular structure in summer. Therefore, if the algorithm detects two events separated by less than 6 h, we consider that this corresponds to the same event.

To provide a cross validation between observations and reanalysis, another jet stream statistic has been obtained using solely the ECMWF reanalysis horizontal winds with the station data. We took the same threshold for the wind speed ($50\,m\,s^{-1}$), and the same criteria on the direction (positive westerly component). However, the temporal and vertical resolutions of VHF and ECMWF are very different: 1 versus 6 h, and 375 m versus 1 km near the tropopause. Thus, we adapted the criteria of ECMWF detection: only one point following the criteria, in time along the vertical, is enough to consider a profile as "jet stream flagged."

c. *Seasonal variability of the jet stream and radionuclide measurements*

As already stated, there is a very large variability of horizontal winds, especially below the tropopause at the altitude of the maximum wind speed, as shown in Figs. 8 and 9. Some of this variability can be attributed to the presence or absence of jet streams over the measurement site. To evaluate the interannual and seasonal variability of the jet stream, we applied the methodology described in the section 4b.

Figure 10 displays the frequency of jet stream events per month. For the two sites, we observe a clear seasonality of the frequency of the jet stream. In winter, the occurrence reaches its peak, between 6.7% and 9.7% in Lannemezan and between 3.5% and 7.8% in Opme. The minimum, near 1%, occurs in June in Lannemezan and May and August in Opme. This result is in agreement with the seasonality of the climatological wind profiles, stronger in winter than in summer. The ECMWF statistic presents the same variations and order of magnitude as the VHF statistic.

The weekly sampling duration of radionuclide measurements is typically not sufficiently time resolved to insure checking for a possible relationship between variations in the radionuclide concentration and the stratosphere–troposphere air exchanges at a given date. However, it is suitable for seasonal variations. Indeed, an overall seasonal variability is also found on radionuclide

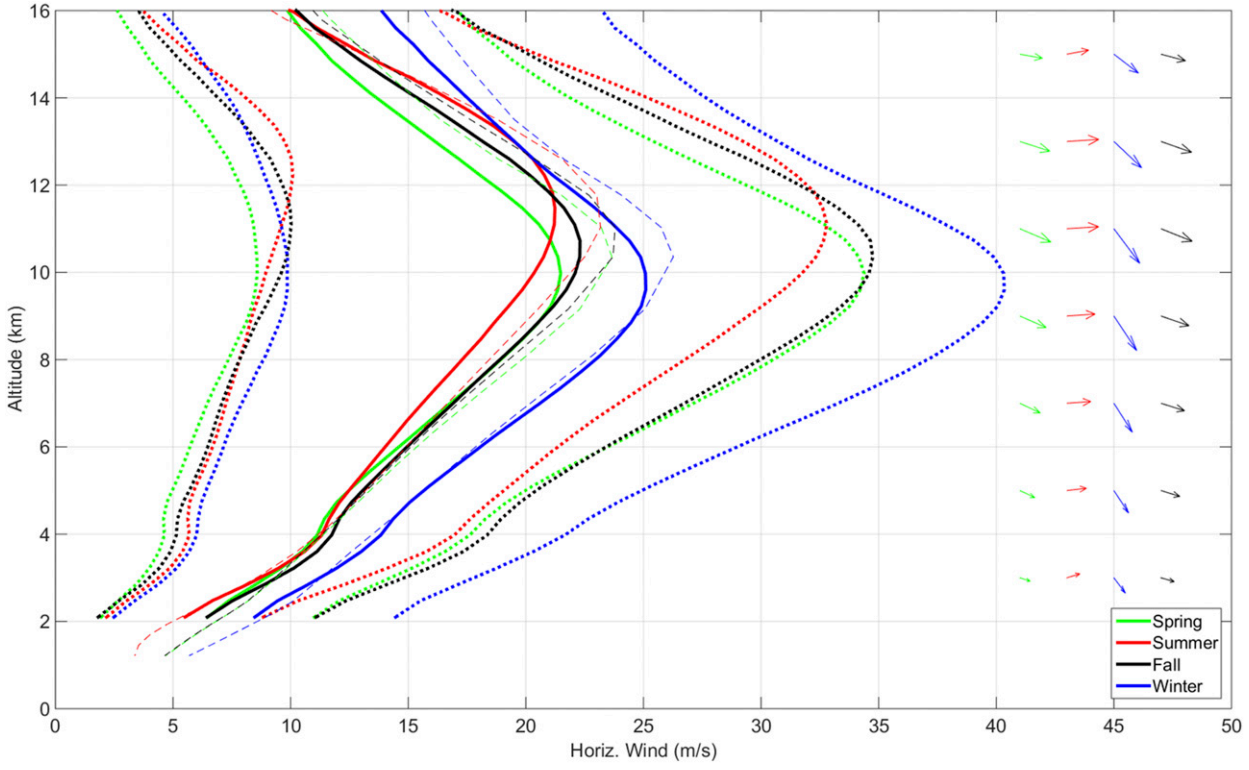

FIG. 9. As in Fig. 8, but for the Lannemezan VHF radar (2001–14).

measurements: a maximum in spring (April–June) and a minimum in autumn–winter can be found for ^{7}Be and ^{22}Na (Fig. 11a). The ^{7}Be spring value in Opme is 1.7 times as high as in autumn. The difference is even more pronounced for ^{22}Na with a 9-yr averaged ratio (spring–winter) of 2.7. This cyclic seasonal structure is typical for Europe and consistent with other seasonal patterns found at many European locations, among them Poland (Błazej and Mietelski 2014), Sicily (Agelao et al. 1984), Serbia (Ajtic et al. 2013), Sweden, or the Czech Republic (Kulan et al. 2006). ^{7}Be is produced roughly 1/3 in the upper troposphere and 2/3 in the stratosphere (Gaggeler 1995). More generally, ^{7}Be activity concentration at a given location provides integrated information on both

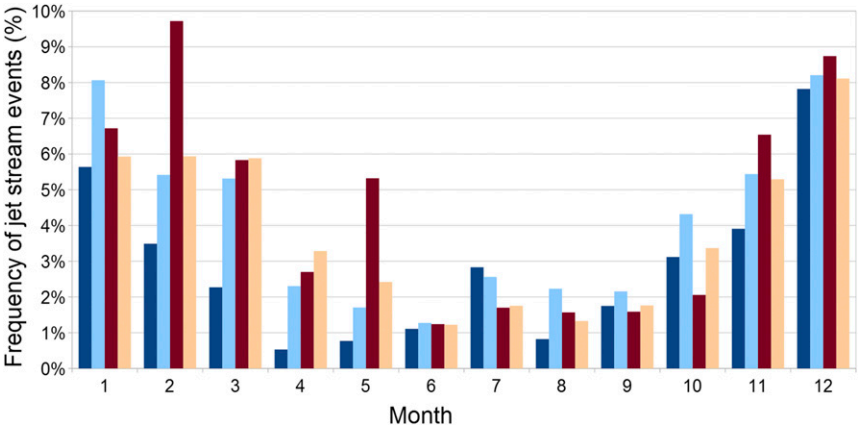

FIG. 10. Monthly frequency (%) of jet stream events at Opme (dark blue: VHF; light blue: ECMWF) and Lannemezan (dark red: VHF; orange: ECMWF). The frequency is obtained by dividing the number of hourly profiles within the jet stream by the total number of profiles produced by the radar systems.

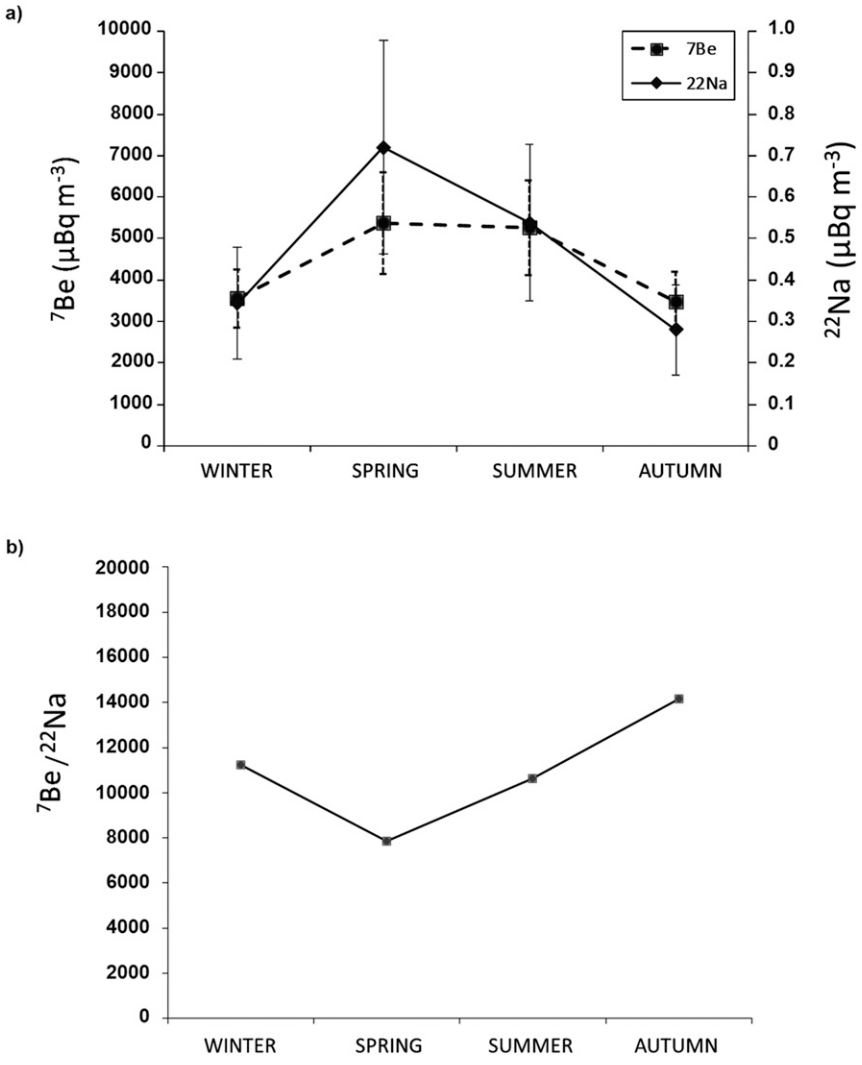

FIG. 11. The 9-yr seasonal variations (a) of average ^{7}Be and ^{22}Na and (b) of the ^{7}Be/^{22}Na ratio in ground-level air at Opme.

production areas and transport (Leppänen et al. 2012). Conversely, ^{22}Na is mostly produced in the upper troposphere and 1/3 in the stratosphere. Therefore, the ^{7}Be/^{22}Na activity ratio can be used to assess the seasonal stratosphere–troposphere air-mass exchange. In the upper troposphere, his ratio is higher than in lower stratosphere. At ground level, this ratio exhibits a seasonal cycle (Fig. 11b). The weekly ^{7}Be/^{22}Na ratio ranges between 4300 and 27 100 while seasonal averages clearly depict lower values in spring and higher values in autumn similarly to what was observed in Poland (Błazej and Mietelski 2014), Finland (Leppänen et al. 2012), or Switzerland (Steinmann et al. 2013).

A low ^{7}Be/^{22}Na ratio indicates a low-stratosphere or upper-troposphere origin. A simultaneous increase of ^{7}Be and decrease of the ^{7}Be/^{22}Na ratio in spring points out the enhanced mixing of lower-stratospheric and/or upper-tropospheric air into the ground-level air (Leppänen et al. 2012; Steinmann et al. 2013). In conclusion, these observations of radionuclide ratio are in agreement with the jet stream seasonality observed over the two sites.

d. Interannual variability and decadal trend of the jet stream

The frequency of jet stream events per year is given in Fig. 12. The Opme yearly series varies between 0.7% (in 2006) and 6.3% (in 2014). The Lannemezan series shows a slightly larger variability, between 0.8% in 2011 and 8.7% in 2010. The mean interannual variability of the frequency of jet stream events is 1.5% in

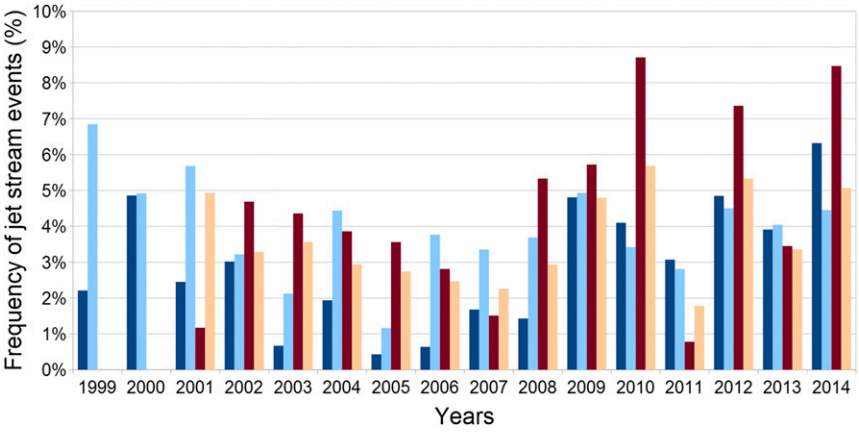

FIG. 12. As in Fig. 10, but for yearly frequency.

Opme and 2.9% in Lannemezan. One can observe quite large differences between the trends calculated from the VHF and ECMWF data after 2010. The trends at Opme, on the contrary, have some large differences in early years but generally seem to agree after 2009. Linear trends have been calculated from monthly occurrence time series for the whole VHF profiler dataset of the two sites, and as function of the seasons (Table 3). The trends are positive and slightly significant in the two sites, $+1.6 \pm 1.2\%$ decade^{-1} for Opme, and $+2.4 \pm 2.2\%$ decade^{-1} for Lannemezan. If we separate the datasets by seasons, the trends are maximum in winter, and significant. For the rest of the year, the trends remain positive, but not significant. The positive trend observed at the two sites is in agreement with a global study based on NCEP–NCAR and ECMWF ERA-40 reanalysis (Strong and Davis 2007). This study shows increased eddy-driven jet core speeds (+15%) and probabilities (+30%) over the midlatitudes, collocated with increases in baroclinicity driven by a spatially heterogeneous pattern of large-scale warming with cooling centers embedded poleward of 60°N. However, these global increasing trends, larger than local trends observed over Opme and Lannemezan in our study, are based on longer series (1958–2007), and present important differences as function of longitude, and also depend on the model used (ERA-40 and NCEP). Barton and Ellis (2009) investigated the variability of the subtropical jet stream without confirming the theory of a general poleward shift in midlatitude jet stream in association with recent climate change, but other recent studies have reported a poleward shift of the jet stream (Rivière 2011; Hudson 2012; Pena-Ortiz et al. 2013). This highlights the need for long-term observation studies of jet stream characteristics and trends.

5. Conclusions

In this study, we used a long series wind measurement from two VHF profilers in France to establish the climatological behavior of upper-tropospheric winds and of the frequency of jet stream events.

First, a case study of jet stream and stratosphere–troposphere exchange occurring in January 2013 was characterized using VHF wind profiler data, water vapor lidar measurements, ERA-Interim, trajectories, and reverse domain-filling calculations.

Then, the climatology study over the two sites revealed that the strongest values of seasonal winds occurred during winter. This wind speed maximum in the upper troposphere is expected to be associated with jet streams, strong eastward winds in the upper troposphere, likely to induce stratosphere–troposphere exchanges of ozone and dry air (Shapiro 1980).

A method of detection of jet stream events has been proposed, and its application on the VHF wind profile series over the two sites shows a clear seasonality of jet stream detection, with a maximum in winter (3.5%–9.7% of hourly profiles) and a minimum in summer (near 1%). Cosmogenic radionuclides sampled in Opme also exhibit a clear seasonal variation

TABLE 3. Linear trends (% decade^{-1}) of the frequency of jet stream events determined from the long series of VHF observations. The confident interval estimate has been estimated using the Student's t distribution at 95% level of confidence.

	Opme	Lannemezan
Whole year	$+1.6 \pm 1.2$	$+2.4 \pm 2.2$
Winter	$+5.6 \pm 3.1$	$+6.9 \pm 5.5$
Spring	$+0.4 \pm 1.1$	$+2.5 \pm 5.3$
Summer	$+0.2 \pm 1.8$	$+0.9 \pm 1.4$
Autumn	$+0.7 \pm 2.6$	$+0.3 \pm 3.4$

with maximum in spring and minimum in the cold seasons while the $^{7}Be/^{22}Na$ activity ratio confirms the stratospheric intrusion for the studied cases. The mean interannual variability of the frequency of the jet stream events is 1.5% in Opme and 2.9% in Lannemezan. We observe positive and slightly significant decadal trends for the two sites ($+1.6 \pm 1.2\%$ decade^{-1} for Opme, and $+2.4 \pm 2.2\%$ decade^{-1} for Lannemezan), maximum in winter ($+5.6 \pm 3.1\%$ decade^{-1} for Opme, and $+6.9 \pm 5.5\%$ decade^{-1} for Lannemezan).

Many studies based on global models describing the long-term global behavior of jet streams have been published. The results are very dependent on the methodology and models used. The current study shows that long series of observations with wind profilers and a regular monitoring of radionuclides are useful to understand the evolution of climate processes, complementing model-related studies. A way to do this could be to link jet stream changes to atmospheric drivers. For instance, Hall et al. (2015) have recently reviewed the possible drivers (cryospheric, oceanic, and stratospheric) of the polar front jet variability. Using wind observations and EOF-based approach in a principal component analysis, several authors investigated the connections between the North Atlantic jet stream and weather regimes such as the North Atlantic Oscillation or the east Atlantic pattern. Athanasiadis et al. (2010) showed that the zonal wind field yield patterns are robust with respect to the range of frequencies included in the data, clearly relate to the position of the climatological mean jets, and are broadly consistent with their traditionally defined counterparts in terms of climatic impacts. Woollings and Blackburn (2012) showed that jet stream changes can be related to leading patterns of variability: the North Atlantic Oscillation and east Atlantic pattern. Future work will aim at linking the long series of French VHF profiler data to the leading patterns influencing weather over Europe.

Acknowledgments. The authors deeply thank the three reviewers and the editor for the constructive comments and useful suggestions. This study has been performed in the framework of ACTRIS-FR (previously SOERE ROSEA/ATMOS). The operation of VHF wind profilers is supported by the Observatoire de Physique du Globe de Clermont-Ferrand/Laboratoire de Météorologie Physique (OPGC/LaMP; http://wwwobs.univ-bpclermont.fr/opgc/index.php) and Observatoire Midi Pyrénées/Laboratoire d'Aérologie [OMP/LA; Pyrenean Platform for Observation of the Atmosphere (P2OA); http://p2oa.aero.obs-mip.fr]. P2OA facilities and staff are funded and supported by the University Paul Sabatier, Toulouse, France, and Centre National de la Recherche Scientifique (CNRS). OPGC/LaMP facilities and staff are funded and supported by the University Clermont-Auvergne, Clermont-Ferrand, France, CNRS, and CNES (EECLAT). We acknowledge the technical staffs of the two observatories, and particularly Patrick Fréville for his work on the lidar instrumentation, and Jean-Marc Pichon for his work at the puy de Dôme station. Guillaume Payen (Reunion Island University) provided the water vapor lidar inversion software. We are grateful to Guillaume Allard for his a preliminary work on the case study during his master training, and to Yahia Gour for useful discussions. We also acknowledge ECMWF for providing ERA-Interim reanalysis.

REFERENCES

Adachi, A., T. Kobayashi, K. Gage, D. Carter, L. Hartten, W. Clark, and M. Fukuda, 2005: Evaluation of three-beam and four-beam profiler wind measurement techniques using a five-beam wind profiler and collocated meteorological tower. *J. Atmos. Oceanic Technol.*, **22**, 1167–1180, doi:10.1175/JTECH1777.1.

Agelao, G., F. Cannizzaro, G. Greco, S. Rizzo, and M. C. Spitale, 1984: Sampling and concentration measurements of ^{7}Be and ^{137}Cs in ground-level air at Palermo. *Health Phys.*, **47**, 96–101.

Ajtić, J. V., D. J. Todorović, J. D. Nikolić, and V. S. Djurdjević, 2013: A multi-year study of radioactivity in surface air and its relation to climate variables in Belgrade, Serbia. *Nucl. Technol. Radiat. Prot.*, **28**, 381–388, https://doi.org/10.2298/NTRP1304381A.

Ancellet, G., J. Pelon, M. Beekmann, A. Papayannis, and G. Mégie, 1991: Ground-based lidar studies of ozone exchanges between the stratosphere and the troposphere. *J. Geophys. Res.*, **96**, 22 401–22 421, doi:10.1029/91JD02385.

Archer, C. L., and K. Caldeira, 2008a: Historical trends in the jet streams. *Geophys. Res. Lett.*, **35**, L08803, https://doi.org/10.1029/2008GL033614.

——, and ——, 2008b: Reply to comment by Courtenay Strong and Robert E. Davis on "Historical trends in the jet streams." *Geophys. Res. Lett.*, **35**, L24807, doi:10.1029/2008GL035114.

Arnold, J., and H. Al-Salih, 1955: Beryllium-7 produced by cosmic rays. *Science*, **121**, 451–453, doi:10.1126/science.121.3144.451.

Athanasiadis, P. J., J. M. Wallace, and J. J. Wettstein, 2010: Patterns of wintertime jet stream variability and their relation to the storm tracks. *J. Atmos. Sci.*, **67**, 1361–1381, doi:10.1175/2009JAS3270.1.

Baray, J.-L., G. Ancellet, F. G. Taupin, M. Bessafi, S. Baldy, and P. Keckhut, 1998: Subtropical tropopause break as a possible stratospheric source of ozone in the tropical troposphere. *J. Atmos. Sol.-Terr. Phys.*, **60**, 27–36, doi:10.1016/S1364-6826(97)00116-8.

——, G. Clain, M. Plu, E. Feld, and P. Caroff, 2010: Occurrence of monsoon depressions in the southwest Indian Ocean: Synoptic descriptions and stratosphere to troposphere exchange investigations. *J. Geophys. Res.*, **115**, D17108, doi:10.1029/2009JD013390.

Barnes, E., and L. Polvani, 2013: Response of the midlatitude jets, and of their variability, to increased greenhouse gases in the CMIP5 models. *J. Climate*, **26**, 7117–7135, doi:10.1175/JCLI-D-12-00536.1.

Barton, N. P., and A. W. Ellis, 2009: Variability in wintertime position and strength of the North Pacific jet stream as represented by re-analysis data. *Int. J. Climatol.*, **29**, 851–862, doi:10.1002/joc.1750.

Bertin, F., B. Campistron, J.-L. Caccia, and R. Wilson, 2001: Mixing processes in a tropopause folding observed by a network of ST radar and lidar. *Ann. Geophys.*, **19**, 953–963, doi:10.5194/angeo-19-953-2001.

Blackburn, M., J. Methven, and N. Roberts, 2008: Large-scale context for the UK floods in summer 2007. *Weather*, **63**, 280–288, doi:10.1002/wea.322.

Błazej, S., and J. W. Mietelski, 2014: Cosmogenic ^{22}Na, ^{7}Be and terrestrial ^{137}Cs, 40K radionuclides in ground level air samples collected weekly in Krakow (Poland) over years 2003–2006. *J. Radioanal. Nucl. Chem.*, **300**, 747–756, doi:10.1007/s10967-014-3049-6.

Bougeault, P., A. Jansa Clar, B. Benech, B. Carissimo, J. Pelon, and E. Richard, 1990: Momentum budget over the Pyrénées: The PYREX experiment. *Bull. Amer. Meteor. Soc.*, **71**, 806–818, doi:10.1175/1520-0477(1990)071<0806:MBOTPT>2.0.CO;2.

Bukunt, B. P., and G. M. Barnes, 2015: The subtropical jet stream delivers the coup de grace to Hurricane Felicia (2009). *Wea. Forecasting*, **30**, 1039–1049, doi:10.1175/WAF-D-15-0004.1.

Caccia, J.-L., and J.-P. Cammas, 1998: VHF-ST radar observations of an upper-level front using vertical and oblique-beam CN2 measurements. *Mon. Wea. Rev.*, **126**, 483–501, doi:10.1175/1520-0493(1998)126<0483:VSROOA>2.0.CO;2.

——, F. Bertin, B. Campistron, V. Klaus, Y. Pointin, J. van Baelen, and R. Wilson, 2000: Cut-off low monitoring by the French VHF-ST-radar network during the ESTIME campaign. *J. Atmos. Sol.-Terr. Phys.*, **62**, 639–651, doi:10.1016/S1364-6826(00)00045-6.

Campistron, B., G. Despaux, M. Lothon, V. Klaus, Y. Pointin, and M. Mauprivez, 2001: A partial 45 MHz sky temperature map obtained from the observations of five ST radars. *Ann. Geophys.*, **19**, 863–871, doi:10.5194/angeo-19-863-2001.

Cattiaux, J., H. Douville, and Y. Peings, 2013: European temperatures in CMIP5: Origins of present-day biases and future uncertainties. *Climate Dyn.*, **41**, 2889–2907, doi:10.1007/s00382-013-1731-y.

Clain, G., J.-L. Baray, R. Delmas, P. Keckhut, and J.-P. Cammas, 2010: A Lagrangian approach to analyse the tropospheric ozone climatology in the tropics: Climatology of stratosphere–troposphere exchange at Reunion Island. *Atmos. Environ.*, **44**, 968–975, doi:10.1016/j.atmosenv.2009.08.048.

Cohen, J., J. Foster, M. Barlow, K. Saito, and J. Jones, 2010: Winter 2009–2010: A case study of an extreme Arctic Oscillation event. *Geophys. Res. Lett.*, **37**, L17707, https://doi.org/10.1029/2010GL044256.

Cristofanelli, P., P. Bonasoni, L. Tositti, U. Bonafé, F. Calzolari, F. Evangelisti, S. Sandrini, and A. Stohl, 2006: A 6-year analysis of stratospheric intrusions and their influence on ozone at Mt. Cimone (2165 m above sea level). *J. Geophys. Res.*, **111**, D03306, doi:10.1029/2005JD006553.

Davini, P., C. Cagnazzo, P. G. Fogli, E. Manzini, S. Gualdi, and A. Navarra, 2014: European blocking and Atlantic jet stream variability in the NCEP/NCAR reanalysis and the CMCC-CMS climate model. *Climate Dyn.*, **43**, 71–85, https://doi.org/10.1007/s00382-013-1873-y.

Dee, D. P., and Coauthors, 2011: The ERA-Interim reanalysis: Configuration and performance of the data assimilation system. *Quart. J. Roy. Meteor. Soc.*, **137**, 553–597, doi:10.1002/qj.828.

Degirmendžić, J., and J. Wibig, 2007: Jet stream patterns over Europe in the period 1950–2001—Classification and basic statistical properties. *Theor. Appl. Climatol.*, **88**, 149–167, doi:10.1007/s00704-006-0237-5.

Diaz de Argandona, J., A. Ezcurra, J. Saenz, B. Campistron, G. Ibarra-Berastegi, and F. Saïd, 2010: Atmospheric tides over the Pyrenees: Observational study and numerical simulation. *Quart. J. Roy. Meteor. Soc.*, **136**, 1263–1274, https://doi.org/10.1002/qj.626

Dritschel, D. G., 1988: Contour surgery: A topological reconnection scheme for extended integrations using contour dynamics. *J. Comput. Phys.*, **77**, 240–266, doi:10.1016/0021-9991(88)90165-9.

Duflot, V., and Coauthors, 2010: Analysis of the origin of distribution of CO in the subtropical southern Indian Ocean in 2007. *J. Geophys. Res.*, **115**, D22106, https://doi.org/10.1029/2010JD013994.

Ecklund, W. L., D. A. Carter, and B. B. Balsley, 1979: Continuous measurement of upper atmospheric winds and turbulence using a VHF Doppler radar: Preliminary results. *J. Atmos. Sol.-Terr. Phys.*, **41**, 983–994, doi:10.1016/0021-9169(79)90099-0.

Feely, H. W., R. J. Larsen, and C. G. Sanderson, 1989: Factors that cause seasonal variations in beryllium-7 concentrations in surface air. *J. Environ. Radioact.*, **9**, 223–249, doi:10.1016/0265-931X(89)90046-5.

Fereday, D. R., A. Maidens, A. Arribas, A. A. Scaife, and J. R. Knight, 2012: Seasonal forecasts of Northern Hemisphere winter 2009/10. *Environ. Res. Lett.*, **7**, 034031, doi:10.1088/1748-9326/7/3/034031.

Freney, E., and Coauthors, 2016: Experimental evidence of the feeding of the free troposphere with aerosol particles from the mixing layer. *Aerosol Air Qual. Res.*, **16**, 702–716, doi:10.4209/aaqr.2015.03.0164.

Fréville, P., and Coauthors, 2015: Lidar developments at Clermont-Ferrand—France for atmospheric observation. *Sensors*, **15**, 3041–3069, doi:10.3390/s150203041.

Fukao, S., M. F. Larsen, M. D. Yamanaka, H. Furukawa, T. Tsuda, and S. Kato, 1991: Observations of a reversal in long-term average vertical velocities near the jet stream wind maximum. *Mon. Wea. Rev.*, **119**, 1479–1489, doi:10.1175/1520-0493(1991)119<1479:OOARIL>2.0.CO;2.

Gäggeler, H. W., 1995: Radioactivity in the atmosphere. *Radiochim. Acta*, **70**, 345–353, https://doi.org/10.1524/ract.1995.7071.special-issue.345.

Haefele, A., M. Hervo, and G. Martucci, 2014: The E-PROFILE network for operational wind, aerosol and cloud observations. *ICAP Sixth Technical Working Group Meeting NWP Applications to Aerosol Forecast and Satellite Verification*, Boulder, CO, International Cooperative for Aerosol Prediction, http://icap.atmos.und.edu/ICAP6/Day2/Haefele_E-PROFILE_.pdf.

Hall, R., R. Erdelyi, E. Hanna, J. M. Jones, and A. A. Scaife, 2015: Drivers of North Atlantic Polar Front jet stream variability. *Int. J. Climatol.*, **35**, 1697–1720, doi:10.1002/joc.4121.

Holton, J. R., P. H. Haynes, M. E. McIntyre, A. R. Douglass, R. B. Rood, and L. Pfister, 1995: Stratosphere-troposphere exchange. *Rev. Geophys.*, **33**, 403–439, doi:10.1029/95RG02097.

Hudson, R. D., 2012: Measurements of the movement of the jet streams at mid-latitudes, in the Northern and Southern Hemispheres, 1979 to 2010. *Atmos. Chem. Phys.*, **12**, 7797–7808, doi:10.5194/acp-12-7797-2012.

Ivanova, A. R., 2016: Stratosphere-troposphere exchange and its specific features at extratropical latitudes. *Russ. Meteor. Hydrol.*, **41**, 170–185, doi:10.3103/S106837391603002X.

Jasiulionis, R., and H. Wershofen, 2005: A study of the vertical diffusion of the cosmogenic radionuclides, ^{7}Be and ^{22}Na in

the atmosphere. *J. Environ. Radioact.*, **79**, 157–169, doi:10.1016/j.jenvrad.2004.06.003.

Kim, K. E., E. S. Jung, B. Campistron, and B. H. Heo, 2001: A physical examination of tropopause height and stratospheric air intrusion—A case study. *J. Meteor. Soc. Japan*, **79**, 1093–1103, doi:10.2151/jmsj.79.1093.

Krishnamurti, T. N., 1961: The subtropical jet stream of winter. *J. Meteor.*, **18**, 172–191, doi:10.1175/1520-0469(1961)018<0172:TSJSOW>2.0.CO;2.

Kuang, X. Y., Y. C. Zhang, Y. Huang, and D. Huang, 2014: Spatial differences in seasonal variation of the upper-tropospheric jet stream in the Northern Hemisphere and its thermal dynamic mechanism. *Theor. Appl. Climatol.*, **117**, 103–112, doi:10.1007/s00704-013-0994-x.

Kulan, A., A. Aldahan, G. Possnert, and I. Vintersved, 2006: Distribution of ^{7}Be in surface air of Europe. *Atmos. Environ.*, **40**, 3855–3868, doi:10.1016/j.atmosenv.2006.02.030.

Leppänen, A. P., I. G. Usoskin, G. A. Kovaltsev, and J. Paatero, 2012: Cosmogenic ^{7}Be and ^{22}Na in Finland: Production, observed periodicities and connection to climatic phenomena. *J. Atmos. Sol.-Terr. Phys.*, **74**, 164–180, doi:10.1016/j.jastp.2011.10.017.

Nastrom, G. D., K. S. Gage, and W. L. Ecklund, 1990: Uncertainties in estimates of the mean vertical velocity from MST radar observations. *Radio Sci.*, **25**, 933–940, doi:10.1029/RS025i005p00933.

Palmin, E., and C. W. Newton, 1948: A study of the mean wind and temperature distribution in the vicinity of the polar front in winter. *J. Meteor.*, **5**, 220–226, doi:10.1175/1520-0469(1948)005<0220:ASOTMW>2.0.CO;2.

Pena-Ortiz, C., D. Gallego, P. Ribera, P. Ordonez, and M. D. C. Alvarez-Castro, 2013: Observed trends in the global jet stream characteristics during the second half of the 20th century. *J. Geophys. Res.*, **118**, 2702–2713, https://doi.org/10.1002/jgrd.50305.

Peters, B., 1959: Cosmic-ray produced radioactive isotopes as tracers for studying large-scale atmospheric circulation. *J. Atmos. Sol.-Terr. Phys.*, **13**, 351–370, doi:10.1016/0021-9169(59)90124-2.

Petitdidier, M., J.-L. Caccia, M. Djebli, V. Klaus, and Y. B. Pointin, 1997: Wind profilers: From PYREX to MAP. *Extended Abstracts, COST-76 Profiler Workshop 1997*, Engelberg, Switzerland, European Commission.

Rao, I., V. Anandan, and P. Reddy, 2008: Evaluation of DBS wind measurement technique in different beam configurations for a VHF wind profiler. *J. Atmos. Oceanic Technol.*, **25**, 2304–2312, doi:10.1175/2008JTECHA1113.1.

Reitebuch, O., C. Lemmerz, E. Nagel, U. Paffrath, Y. Durand, M. Endemann, F. Fabre, and M. Chaloupy, 2009: The airborne demonstrator for the direct-detection Doppler wind lidar ALADIN on ADM-Aeolus. Part I: Instrument design and comparison to satellite instrument. *J. Atmos. Oceanic Technol.*, **26**, 2501–2515, doi:10.1175/2009JTECHA1309.1.

Rivière, G., 2011: A dynamical interpretation of the poleward shift of the jet streams in global warming scenarios. *J. Atmos. Sci.*, **68**, 1253–1272, doi:10.1175/2011JAS3641.1.

Schaefer, V., 1953: Cloud forms of the jet stream. *Tellus*, **5**, 27–31, doi:10.1111/j.2153-3490.1953.tb01032.x.

Shapiro, M. A., 1980: Turbulent mixing within tropopause folds as a mechanism for the exchange of chemical constituents between the stratosphere and troposphere. *J. Atmos. Sci.*, **37**, 994–1004, doi:10.1175/1520-0469(1980)037<0994:TMWTFA>2.0.CO;2.

Staley, D., 1960: Evaluation of potential vorticity changes near the tropopause and the related vertical motions, vertical advection of vorticity, and transfer of radioactive debris from the stratosphere. *J. Meteor.*, **17**, 591–620, https://doi.org/10.1175/1520-0469(1960)017<0591:EOPVCN>2.0.CO;2.

Steinmann, P., M. Zeller, P. Beuret, G. Ferreri, and S. Estier, 2013: Cosmogenic ^{7}Be and ^{22}Na in ground level air in Switzerland (1994–2011). *J. Environ. Radioact.*, **124**, 68–73, doi:10.1016/j.jenvrad.2013.03.012.

Strauch, R., B. Weber, A. Frisch, C. Little, D. Merritt, K. Moran, and D. Welsh, 1987: The precision and relative accuracy of profiler wind measurements. *J. Atmos. Oceanic Technol.*, **4**, 563–571, doi:10.1175/1520-0426(1987)004<0563:TPARAO>2.0.CO;2.

Strong, C., and R. E. Davis, 2007: Winter jet stream trends over the Northern Hemisphere. *Quart. J. Roy. Meteor. Soc.*, **133**, 2109–2115, doi:10.1002/qj.171.

——, and ——, 2008: Comment on ''Historical trends in the jet streams'' by Cristina L. Archer and Ken Caldeira. *Geophys. Res. Lett.*, **35**, L24806, doi:10.1029/2008GL034829.

Thomas, L., R. J. Winder, and R. Rüster, 1986: The characteristics of VHF radar echoes from the tropopause region near a jet stream. *J. Atmos. Sol.-Terr. Phys.*, **48**, 261–265, doi:10.1016/0021-9169(86)90100-5.

Tokuyama, H., and S. Igarashi, 1998: Seasonal variation in the environmental background level of cosmic-ray-produced 22Na at Fukui City, Japan. *J. Environ. Radioact.*, **38**, 147–161, doi:10.1016/S0265-931X(97)88739-5.

Trickl, T., N. Bärtsch-Ritter, H. Eisele, M. Furger, R. Mücke, M. Sprenger, and A. Stohl, 2011: High-ozone layers in the middle and upper troposphere above central Europe: Potential import from the stratosphere along the subtropical jet stream. *Atmos. Chem. Phys.*, **11**, 9343–9366, doi:10.5194/acp-11-9343-2011.

Woollings, T., and M. Blackburn, 2012: The North Atlantic jet stream under climate change and its relation to the NAO and EA patterns. *J. Climate*, **25**, 886–902, doi:10.1175/JCLI-D-11-00087.1.

Yoe, J. O., and R. Rüster, 1992: VHF Doppler radar observations of vertical velocities in the vicinity of the jet stream. *Mon. Wea. Rev.*, **120**, 2378–2382, doi:10.1175/1520-0493(1992)120<2378:VDROOV>2.0.CO;2.